Calculation of the effective diffusivity of heterogeneous media using the lattice-Boltzmann method

José Alvarez-Ramírez,* Salvador Nieves-Mendoza, and Jesús González-Trejo†
División de Ciencias Básicas e Ingenieria, Universidad Autónoma Metropolitana, Campus Iztapalapa, Apartado Postal 55-534, 09000 México Distrito Federal, Mexico
(Received 30 March 1995)

The effective diffusivity of a heterogeneous medium is calculated numerically as a function of the inclusion fraction using the lattice-Boltzmann approach. Effective diffusivities are calculated for structures consisting of either permeable or nonpermeable inclusions distributed in a continuous phase. Two-dimensional simulations show good agreement with results obtained by means of Monte Carlo simulations of tracer diffusion. Numerical results are shown that are in agreement with the predictions of Maxwell's equation, for small inclusion fractions.

PACS number(s): 51.10.+y, 66.30.Jt, 05.60.+w

I. INTRODUCTION

Diffusion in heterogeneous media is a central issue in a wide variety of mass transfer phenomena. Transport of methane in coal beds [1], diffusion of reactive substances in catalizers [2], and transport of nutrients in tissues [3] are examples that are intimately involved with diffusion in heterogeneous media. These systems are often composed of one or more dispersed phases distributed in a single continuous phase. In general, the effective diffusivity of molecules through heterogeneous materials depends on the inclusion fraction and solute mobility in each phase as well as on morphological details of the individual phases [4,5].

Consider a heterogeneous medium with either permeable or nonpermeable inclusions. A concentration gradient is applied across the medium maintaining steady mass transport (see the "experimental setup" in Fig. 1). The mass transport is locally described by the diffusion equation

$$\frac{\partial \rho}{\partial t}-\nabla(D_P\nabla\rho)=0\ . \tag{1}$$

Here ρ is the molar concentration, and D_P is the local molecular diffusivity, which is equal to D_C in the continuous phase and D_I in the inclusion phase. If the inclusion phase is nonpermeable, then $D_I=0$. At length scales much larger than the typical pore size, the mass transport in Fig. 1 is generally described by the macroscopic diffusion equation [4]

$$\frac{\partial C}{\partial t}-D_{\text{eff}}\nabla^2 C=0\ , \tag{2}$$

where C is the macroscopic mean concentration, and D_{eff} is the effective diffusivity coefficient along the $\mathbf{X}_1$ direction. The coefficient D_{eff} can be defined as follows: let w^* and w be the steady-state molar flux across the heterogeneous media and the homogeneous media (no inclusion phase), respectively. Then D_{eff} is given by the following relation [4]:

$$D_{\text{eff}}=\frac{w^*}{w}D_c\ . \tag{3}$$

That is, D_{eff} is the number that fits the macroscopic Fick's law $w^*=D_{\text{eff}}G$, where G is the steady-state gradient for the homogeneous media case. One can show that

$$w=D_C(\rho_2-\rho_1)L_2/L_1$$

and

$$w^*=\int_0^{L_2} D_P(\partial\rho/\partial\mathbf{X}_1)_{\mathbf{X}_1=L_1}d\mathbf{X}_2\ .$$

So that, in order to calculate w^*, the steady-state concentration distribution $\rho(\mathbf{X}_1,\mathbf{X}_2)$ must be known. This is achieved by solving the steady state in (1) with suitable boundary conditions (no mass flux at nonpermeable boundaries, and constant concentrations at right and left

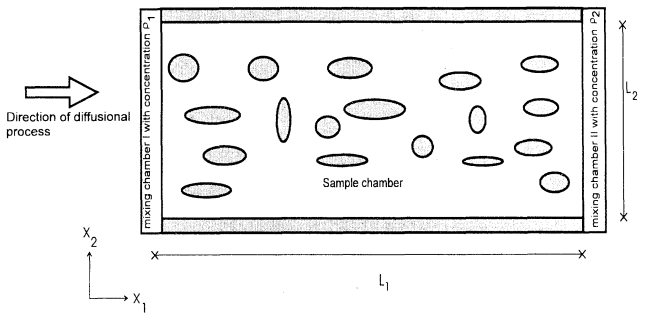

FIG. 1. Experimental setup for the estimation of effective diffusivities.

*Electronic address: jjar@xanum.uam.mx
†Also at Campus Azcapotzalco.

boundaries).

Previous approaches concerning prediction of D_{eff} in multiphase materials include Monte Carlo simulation of tracer molecules [5] and methods of volume averaging [4]. In the former approach, tracer particles undergo a simulated random walk through the structure of a heterogeneous material. Molecular diffusion in the continuous phase is described as a series of randomly directed steps, with length $\lambda=\lambda_0 \ln\varepsilon$, where $\varepsilon\in[0,1]$ is a random number and λ_0 is a mean step length. The effective diffusivity is calculated by monitoring the distance traveled by the tracers in a certain amount of time. The diffusivity is calculated using the relationship [5]

$$D_{\text{eff}}=\frac{\langle \mathbf{X}^2\rangle}{2d\sum\lambda} ,$$

where $\langle \mathbf{X}^2\rangle$ is the mean-squared displacement, d represents the dimensionality of the system, and $\sum\lambda$ is the total length of the walk. Because of its stochastic nature, Monte Carlo simulations need a large amount (of the order of 10^4) of tracer particles to obtain accurate estimates of diffusivities. In the method of volume averaging, one departs from the diffusion equation defined on a heterogeneous domain with suitable boundary conditions [4]. If spatially periodic heterogeneous media are assumed and variations on local diffusivities within the periodic cell are neglected, it is possible to take volume averaging of the continuity equation to obtain a representation of the transport equations with no geometry limitations [4]. The main advantage of this procedure in comparison with other approaches is that an algorithm for the calculation of the tensor of effective transport coefficients is obtained. However, the volume averaging approach has the limitations of being restricted to spatially periodic media. Kim, Ochoa, and Whitaker [4] compared effective diffusivities predicted with the volume averaging procedure and experimental diffusivities in transversal isotropic, unconsolidated porous media. Such comparison between theory and experiment showed good agreement and clearly indicated the influence of the global structure on the effective transport coefficients. Measurements were made in physical systems consisting of glass spheres, mica particles, and disks made from Mylar sheets.

In a recent work, Garbuczi and Bentz [6] used the Nerst-Einstein relation, which connects the electrical conductivity of the material with its diffusivity, to estimate effective diffusivities of cement-based materials. By imposing a voltage gradient across the sample, the estimation problem is reduced to the solution of a conductor network mapping problem, which is solved via conjugate gradient relaxation algorithm. Essentially, one solves the complete electrical problem of the voltage distribution in a random material across which a potential difference is applied.

The extension of the above-discussed methods to systems with rather complex transport phenomena including chemical reaction, adsorption, etc., is not straightforward. Heterogeneous media including fluid flow and chemical reactions are common in physical situations. In principle, an alternative to address this class of problems is to solve the transport equations [4,5] to obtain information concerning effective transport coefficients [as posed by Eqs. (1) and (3) for D_{eff}].

In this work, we describe a lattice-Boltzmann (LB) method [7–11] to determine D_{eff} as defined by Eq. (3). It has recently been shown that LB methods provide alternative numerical techniques for solving transports equations, such as the Navier-Stokes [8] and reaction-diffusion systems [9]. The parallel nature of these newly developed schemes, adapted from cellular automata, affords an easy implementation of fast, efficient, and accurate simulations in parallel machines [8]. The efficiency of the LB methods competes with that of traditional numerical methods, while their physical interpretation is transparent [7]. For instance, nonpermeable boundaries are implemented via the classical bounce back boundary condition of lattice-gas simulations.

The basic idea for the calculation of D_{eff} is the following: for a given heterogeneous medium with either permeable or nonpermeable inclusions, find the steady-state solution of (1) via the LB numerical scheme; then calculate the mass flux w across the right (or left) boundary (see Fig. 1) to estimate the relative diffusivity $D_r=D_{\text{eff}}/D_C$ by means of Eq. (3). Estimates of D_{eff} obtained in this work agree very well with those obtained with Monte Carlo simulations [5] for permeable inclusions. On the other hand, results from LB simulations are compared with predictions from the Maxwell's equations [12], showing good agreement for small inclusions fractions. As in previous work [4,5], it is found that the morphological details of the heterogeneous media have an important effect on the behavior of D_{eff} with respect to the inclusion fraction.

The work is organized as follows. Section II describes the LB method. Section III discusses the numerical strategy to implement the LB algorithm. Finally, Sec. IV presents and discusses results of simulations.

II. THE LATTICE-BOLTZMANN METHOD

A lattice gas is a simplified model of molecular dynamics. It is a fully discretized model in which a regular lattice is populated by identical, pointlike particles positioned on the nodes. The particles propagate along the lattice links and interaction with each other only when they meet at a node. Then a collision occurs, conserving mass. After the collision the particles are redistributed in the available lattice directions. Lattice-gas methods have proven to be useful in many applications such as flow [7–9] and phase transition [11] simulations. Lattice gases are especially suitable for treating complicated boundary conditions and complex domains, because no slip and no transport boundary conditions are easily implemented (it lets the particles bounce and back).

In the LB method, instead of using discrete particles,

one describes the time evolution of population densities assuming Boltzmann distribution locally [7,8]. The LB method discussed has the following characteristic: a regular, square lattice, L, suspended in two-dimensional space, $\Omega=[0,L_1]\times[0,L_2]$, with four links per node, each link having unit length ΔX, and time advances in units of ΔT, where L and T are spatial and temporal scale lengths, respectively. Let $f_i(\mathbf{x},t)$ be the one-particle distribution function with velocity $\mathbf{e}_i$ at some dimensionless time t and dimensionless position $\mathbf{x}$. The nearest-neighbor vectors are taken as

$$\mathbf{e}_i=\cos\left[\frac{(i-1)\pi}{2}\right]\mathbf{u}_1+\sin\left[\frac{(i-1)\pi}{2}\right]\mathbf{u}_2,\quad 1\le i\le 4\ ,$$

where $\mathbf{u}_1$, $\mathbf{u}_2$ are unit vectors along the x_1 and x_2 directions, respectively. In addition, a rest particle state ($\mathbf{e}_0=\mathbf{0}$) is used. Consequently at each lattice site, we have five states. The behavior of a LB method is governed directly by its rules: rules for advecting particles to new locations and rules for determining the new directions of the particles. These are characterized in the microdynamical evolution equation as [7,8]

$$f_i(\mathbf{x}+\mathbf{e}_i,t+1)-f_i(\mathbf{x},t)=\Omega_i(\mathbf{x},t)\ , \tag{4}$$

where Ω_i is the collision operator. The zeroth moment (total mass) at time t and position $\mathbf{x}$, is defined by

$$\rho(\mathbf{x},t)=\sum_{j=0}^{4} f_j(\mathbf{x},t) \tag{5}$$

if the transport (diffusion) equation is written in physical coordinates $(\mathbf{X},T)$ as follows:

$$\frac{\partial\tilde{\rho}}{\partial t}-\nabla(\tilde{D}\nabla\tilde{\rho})=0\ , \tag{6}$$

where $\tilde{D}$ is the physical diffusion coefficient. Then coordinates $(\mathbf{x},t)$ are related to $(\mathbf{X},T)$ coordinates by $\mathbf{X}_j=\mathbf{x}_j\Delta x$ and $T=t\Delta t$, and lattice density ρ and physical density $\tilde{\rho}$ are related by $\rho=\tilde{\rho}(\Delta x)^2$. If the system is close to equilibrium, the collision operator, $\Omega_i(\mathbf{x},t)$ can be linearized about a local equilibrium distribution. After the linearization, Ω_i appears as a matrix acting upon the deviations of $f_i(\mathbf{x},t)$ from its equilibrium $f_i^{\mathrm{eq}}(\mathbf{x},t)$, such that Eq. (4) takes the form [8]

$$f_i(\mathbf{x}+\mathbf{e}_i,t+1)-f_i(\mathbf{x},t)$$

$$=\sum_{j=0}^{4}\Omega_{ij}[f_j(\mathbf{x},t)-f_i^{\mathrm{eq}}(\mathbf{x},t)]\ . \tag{7}$$

In addition, it can be taken $\Omega_{ij}=-\delta_{ij}/\tau$ (uncorrelated collision redistribution), which is known as the single relaxation time (Bernstein-Green-Kruskal) approximation [7]. We obtain the equilibrium solutions by imposing a Boltzmann distribution locally:

$$f_i^{\mathrm{eq}}(\mathbf{u})=f_i^{\mathrm{eq}}(\mathbf{0})Ze^{\langle\mu,e_i\rangle},\quad f_0^{\mathrm{eq}}(\mathbf{u})=f_0^{\mathrm{eq}}(\mathbf{0})\ , \tag{8}$$

where u is the velocity at the node and Z is the partition function given by

$$Z=\frac{1}{f_0^{\mathrm{eq}}(\mathbf{0})+\sum_{i=1}^{4} f_i^{\mathrm{eq}}(\mathbf{0})e^{\langle\mu,\mathbf{e}_i\rangle}}$$

where μ is a velocity-dependent term, and $\langle\ ,\ \rangle$ denotes the standard internal product. For $\mathbf{u}=\mathbf{0}$ (our case), it is possible to conclude that $\mu=0$ [8]. Therefore

$$f_i^{\mathrm{eq}}(\mathbf{x},t)=\frac{\rho(\mathbf{x},t)-f_0^{\mathrm{eq}}(\mathbf{x},t)}{4},\quad i\neq 0. \tag{9}$$

One can show that $f_i^{\mathrm{eq}}(\mathbf{x},t)=\rho(\mathbf{x},t)/8$ and $f_0^{\mathrm{eq}}(\mathbf{x},t)=\rho(\mathbf{x},t)/2$ [8]. The transition to a continuum description is done by assuming that the $f_i\ (\mathbf{x},t)$ have appreciable variations only over a space scale $L_i\gg\Delta X$ and a time scale $T\gg\Delta T$. Ponce-Dawson, Chen, and Doolen [9] developed the mapping of the LB equations (7)–(9) to the diffusion equation (6) for a triangular lattice. Although the procedure is essentially the same as that in [9], for the sake of completeness in presentation we will derive the LB diffusion equation for a square lattice. The left-hand side of Eq. (4) can be replaced by its Taylor expansion, to yield a differential form of the LB equation:

$$\sum_{n=1}^{\infty}\frac{1}{n!}(\varepsilon^2\partial_t+\varepsilon\langle\mathbf{e}_i\cdot\partial_{\mathbf{x}}\rangle)^n f_i(\mathbf{x},t)=\Omega_i(\mathbf{x},t)\ , \tag{10}$$

where $\partial_t=\partial/\partial t$, $\partial_{\mathbf{x}}=(\partial/\partial\mathbf{x}_1,\partial/\partial\mathbf{x}_2)$. In the above expression, the following scalings have been assumed [9]: $f_i=O(\varepsilon)$, $\partial_t=O(\varepsilon^2)$, and $\partial_x=O(\varepsilon)$, where ε is a small parameter. In fact, *since* the purpose of the model is to describe diffusion effects, we have $\Delta X/L_i=O(\varepsilon)$ and $\Delta T/T=O(\varepsilon^2)$. Up to second order ($n=2$), Eq. (10) becomes

$$\varepsilon^2\partial_t f_i+\varepsilon\langle\mathbf{e}_i\cdot\partial_{\mathbf{x}}\rangle f_i+\frac{\varepsilon^2}{2}\mathbf{e}_i^T\partial_{\mathbf{x}}^2 f_i(\mathbf{x},t)\mathbf{e}_i$$

$$=-\frac{[f_i(\mathbf{x},t)-f_i^{\mathrm{eq}}(\mathbf{x},t)]}{\tau}\ . \tag{11}$$

We assumed that $f_i(\mathbf{x},t)$ has small departure from equilibrium $f_i^{\mathrm{eq}}(\mathbf{x},t)$:

$$|f_i(\mathbf{x},t)-f_i^{\mathrm{eq}}(\mathbf{x},t)|\ll f_i^{\mathrm{eq}}(\mathbf{x},t)\ .$$

So that $f_i(\mathbf{x},t)$ can be written as

$$f_i(\mathbf{x},t)=f_i^{\mathrm{eq}}(\mathbf{x},t)+\varepsilon f_i^1(\mathbf{x},t)+O(\varepsilon^2)\ ,$$

where f_i^1 has to be determined. Then, Eq. (11) can be split into two parts corresponding to ε and ε^2 variations:

$$\langle\mathbf{e}_i^T\cdot\partial_{\mathbf{x}}\rangle f_i^{\mathrm{eq}}=-\frac{f_i^1}{\tau}\quad(\varepsilon)\ , \tag{12}$$

$$\partial_t f_i^{\mathrm{eq}}+\langle\mathbf{e}_i^T\cdot\partial_{\mathbf{x}}\rangle f_i^1+\tfrac{1}{2}\mathbf{e}_i^T\partial_{\mathbf{x}}^2 f_i\mathbf{e}_i=0\quad(\varepsilon^2)\ . \tag{13}$$

From (9), the following equality is obtained

$$f_i^1 = -\tau \langle \mathbf{e}_i \cdot \partial_{\mathbf{x}} \rangle f_i^{\mathrm{eq}} . \quad (14)$$

The above equation can be interpreted as an analogy to the Fick law of mass transport [13] where f_i^1 is the mass flux in the ith direction and τ is the "diffusion coefficient." Substitution of (14) into (13) yields

$$\partial_t f_i^{\mathrm{eq}} - \mathbf{e}_i^T \partial_{\mathbf{x}} [\tau \langle \mathbf{e}_i \cdot \partial_{\mathbf{x}} \rangle f_i^{\mathrm{eq}}] + \tfrac{1}{2} \mathbf{e}_i^T \partial_{\mathbf{x}}^2 f_i \mathbf{e}_i = 0 . \quad (15)$$

Summing over i and taking into account the isotropy of the second-order term $\sum_i e_{ij} e_{jk} = 2\delta_{ik}$, we get

$$\partial_t \rho - \nabla (D \nabla \rho) = 0 , \quad (16)$$

where $D = \frac{1}{2}(\tau - \frac{1}{2})$ is the diffusivity coefficient of the lattice, which is related to the physical diffusivity coefficient $\tilde{D}$ by

$$D = \tilde{D} \frac{(\Delta T)}{(\Delta X)^2} = \tfrac{1}{2}(\tau - \tfrac{1}{2}) . \quad (17)$$

Note that the lattice parameter τ ranges from $+0.5$ to infinity. However, it is known that the single relaxation time approach is a good approximation only for values of τ ranging from 0.5 to around 10 [9]. Given a physical diffusivity coefficient $\tilde{D}$, a relaxation time τ, and a lattice spacing ΔX, the second equality in (17) defines the actual time step ΔT. If the diffusivity coefficient $\tilde{D}$ varies with position $\mathbf{x}$, one merely chooses τ as a function of $\mathbf{x}$ according to (17).

In calculations of fluid flow using LB methods, it is well known that the square lattice does not have proper isotropy of fourth-order tensors [8]. However, in calculations of mass diffusion the use of the square lattice it is not a problem since only isotropy of second-order tensors (like $\sum_i e_{ij} e_{jk}$) is sufficient to derive the diffusion equation (6).

III. NUMERICAL STRATEGY

This paper focuses on diffusion through two-dimensional heterogeneous media constructed by placing inclusions in a continuous phase (see Fig. 1).

Because in each phase different diffusivities are assigned (or different LB parameter τ), it is necessary to know at all times the location of the phases. To accomplish this, the simulation domain is discretized into a logical matrix array of nodes (typically, 500×500 for two-dimensional simulations). The lattice is used only to discretize the spatial structure; distribution of phase nodes can be made randomly or deterministically. The inclusions have maximum diameter 50, in units of lattice spacing. Nodes belonging to the inclusion phase are assigned a logical value .TRUE., and all other nodes are assigned .FALSE. To determine the phase in which the transport phenomenon is taking place, the algorithm recalls the value of the node; a returned value of .TRUE. means the mass is inside an inclusion, while a value of [5], the above discretization procedure is flexible and can be used to investigate both regular (maybe periodic) or irregular inclusion geometries. In simulations the mass is kept diffusing by imposing a difference concentration across the media. For each configuration of inclusions, the system was allowed to attain the steady-state and then the mass flux measurements were averaged over the next 5000 time steps. Because the first-order approximation (11) works well for small values of τ, we have used $\tau = 1$ for the continuous phase in all the simulations.

To simulate nonpermeable inclusions, the standard bounce back boundary condition [7–9] was implemented in the boundary between permeable and nonpermeable regions. To simulate permeable inclusions, mass is translated across the boundary between regions with different diffusion coefficients, and collision step [Eq. (7)] is carried out according with the value of τ [calculated as in (17)] corresponding to the node. Specifically, $\tau = 2D_C + \frac{1}{2}$ if the node belongs to the continuous phase (.TRUE.), and $\tau = 2D_I + \frac{1}{2}$ if the node belongs to the inclusion phase (.FALSE.). In this way the current is conserved across the boundary between regions with different diffusion coefficient.

IV. NUMERICAL RESULTS

We present two sets of numerical simulations that describe diffusion in heterogeneous media with permeable inclusions, and diffusion through heterogeneous media with nonpermeable inclusions.

Effective diffusivity results for overlapping rectangular inclusions in two dimensions are presented in Fig. 2. Results are reported as relative diffusivities $D_r = D_{\mathrm{eff}}/D_C$ for inclusion fractions in the range $0 \le \varphi \le 1$ and diffusivity ratios D_C/D_I ranging from 1.25 to 4.0. Inclusions are randomly distributed rectangles with sides aligned with the coordinates axis $\mathbf{X}_1$ and $\mathbf{X}_2$. If r_1 and r_2 are the size of such rectangles, then r_1 ranges from 1 to 5 spatial lattice units and $0.25 \le r_1/r_2 \le 5.0$. Each point in Fig. 2 represents the average of five structural realizations to a given inclusion fraction. We have also included the values predicted by the Maxwell's equation [12]:

$$D_r = \frac{2D_C + D_I - 2\varphi(D_C - D_I)}{2D_C + D_I + \varphi(D_C - D_I)} , \quad (18)$$

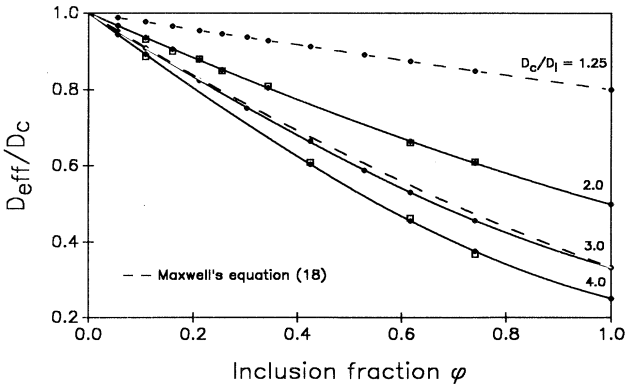

FIG. 2. Effective diffusivities for overlapping and permeable rectangular inclusions. Open square symbols represent Monte Carlo results.

which was derived assuming that the inclusion phase occupies a small fraction and consists of nonoverlapping, spherical inclusions randomly distributed in the continuous phase. Notice that, results from LB simulations and predictions from Maxwell's equation (18) agree very well, for small ratios D_C/D_I and all inclusion fractions. Such agreement leads to the conclusion that Maxwell's equation is also valid for nonspherical inclusions. To compare with Monte Carlo techniques, we calculated the relative diffusivity by means of the method reported in [5]. Tracer particles undergo a simulated random walk through the structural representation. Here molecular diffusion in the continuous phase is described as a series of randomly directed steps with length $\lambda=\lambda_0 \ln\varepsilon$, where ε is a random number with uniform probability in [0,1], and λ_0 is the mean step length in the continuous phase. Particles inside the inclusions take steps of length $\lambda=-\gamma\lambda_0\ln\varepsilon$, where $\gamma=D_I/D_C$ [5]. In this way, the current is conserved across the boundary between regions with different diffusion coefficients. Results show good agreement between effective diffusivities obtained via Monte Carlo and LB techniques.

Although we have obtained results only for the inclusion geometry described above, the technique can be used to investigate a wide variety of inclusion geometries, such as spheres and irregularly shaped inclusions. We consider now the case of nonpermeable inclusions. Because mass transfer takes place only in the continuous phase, a diffusion problem with complex boundaries must be solved. No mass flux across inclusion boundaries is easily implemented. One merely lets particles bounce off neighboring nodes defining the inclusion boundary. Figure 3 shows a typical concentration distribution for overlapping rectangular inclusions with $r_1/r_2=0.5$. The concentration scale can be read according with the color scale at the right of the figure, and inclusions are represented in black color. Figure 4 shows results of effective diffusivities for randomly distributed inclusions (as in Fig. 3) with rectangular geometry for the rates $r_1/r_2=0.5$ and $r_1/r_2=2.0$. Note that the effective diffusivity in the case $r_1/r_2=2.0$ is higher than the

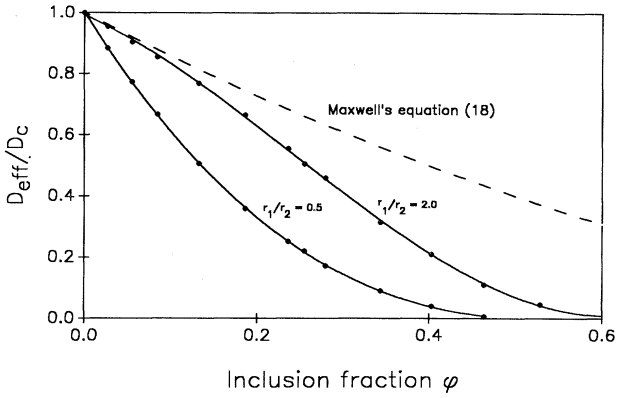

FIG. 4. Effective diffusivities for randomly distributed inclusions with rectangular shape.

effective diffusivity in the case $r_1/r_2=0.5$. This is a consequence of the fact that, for $r_1/r_2=2.0$, the inclusions are aligned with the direction of the diffusional process, such that preferential channels of transport are created. On the other hand, for $r_1/r_2=0.5$, the inclusions are orthogonally aligned with the direction of transport, such that they oppose the diffusional process. Following the notation in Kim, Ochoa, and Whitaker's work [4], the curves in Fig. 4 corresponding to the $r_1/r_2=2.0$ and $r_1/r_2=0.5$ cases represent the two distinct components of the effective diffusivity tensor in transversely isotropic, unconsolidated porous media. The difference between such effective diffusivities illustrates the fact that the randomly distributed rectangular inclusion induces an anisotropic media. The ratio between the effective diffusivities in Fig. 4 ranges from 1.0 to 3.0, which is in accord with the ranges derived via volume averaging techniques for spatially periodic inclusions [4]. Figure 4 also includes the relative diffusivities D_r predicted with Maxwell's equation (18). As expected from Maxwell's assumptions, predictions of LB techniques and

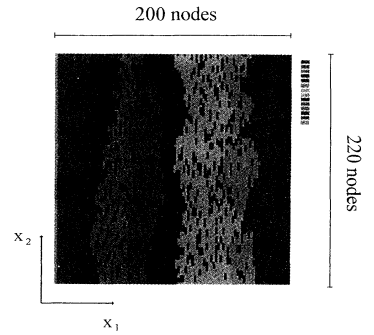

FIG. 3. Typical concentration distribution for the case of nonpermeable inclusions. Concentrations are displayed according with the scale at the right-hand side of the figure.

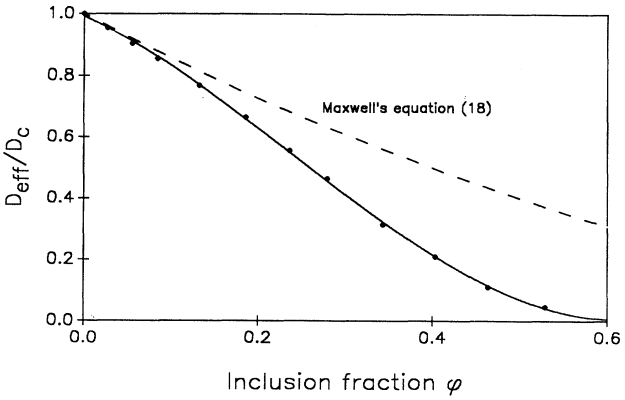

FIG. 5. Effective diffusivities for randomly distributed nonpermeable ellipsoids.

Maxwell's equation agree well for small inclusion fractions ($0 \leq \varphi \leq 0.15$), however, such agreement is better for the $r_1/r_2 = 2.0$ case. Observe that there exists a critical inclusion fraction $\varphi^* < 1.0$ for which $D_{\text{eff}} = 0$, where φ^* depends mainly on the inclusion geometry. φ^* is a threshold inclusion fraction at which there is not mass transport across the sample. In other words, at φ^* the accessible porosity of the porous media becomes equal to zero [5].

Finally, Fig. 5 shows the behavior of D_r with respect to inclusion fraction φ for two-dimensional spheroids randomly distributed in a continuous phase. The shape of the curve (D_r, φ) is the same as the ones in Fig. 4: namely, a smooth decaying followed by an inaccessible structure ($D_r \rightarrow 0$) depending on the inclusion geometry. This suggests the existence of a universal behavior, in analogy with the permeability of fluids in porous media [14].

V. CONCLUSIONS

We have presented in this paper a numerical strategy that uses LB techniques to estimate effective diffusivities in heterogeneous media. The LB techniques are easily implementable because of their ability to handle complicated domains arising from heterogeneous media cases. Results were illustrated for structures consisting of rectangles or spheres randomly distributed in a continuous phase of lower diffusivity; however, our methodology can be used to study any type of structure. Because LB techniques can describe diffusional processes in non-steady-state regime, it can be used to describe dynamic effective diffusivities of heterogeneous media [14]. This work is now in progress. Also a study of spatially periodic structures and its comparison with volume averaging procedure results will be presented elsewhere.

ACKNOWLEDGMENT

Two of us (S.N.M. and J.G.T.) would like to thank CONACyT for financial support.

[1] D. M. Smith and F. L. Williams, Soc. Petroleum Eng. J. **24**, 529 (1984); R. Jackson, *Transport in Porous Catalysts* (Elsevier, New York, 1977).

[2] N. Wakao and J. M. Smith, Chem. Eng. Sci. **17**, 825 (1962).

[3] B. A. Westrin and A. Axelsson, Biotechnol. Bioeng. **38**, 439 (1991).

[4] J. H. Kim, J. A. Ochoa, and S. Whitaker, Transp. Porous Media **2**, 327 (1987).

[5] M. R. Riley, F. J. Muzzio, H. M. Buettner, and S. C. Reyes, Phys. Rev. E **49**, 3500 (1994); S. Reyes and K. F. Jensen, Chem. Eng. Sci. **40**, 1723 (1985).

[6] E. J. Garbuczi and D. P. Bentz, J. Mat. Sci. **27**, 2083 (1992).

[7] F. Higuera, S. Succi, and R. Benzi, Europhys. Lett. **9**, 345 (1989).

[8] R. D. Kingdom, P. Schofield, and L. White, J. Phys. A **25**, 3559 (1992); F. J. Alexander, S. Chen, and J. D. Sterling, Phys. Rev. E **47**, R2249 (1993); D. Grunau, S. Chen, and K. Eggert, Phys. Fluids A **5**, 2557 (1993).

[9] S. Ponce-Dawson, S. Chen, and G. D. Doolen, J. Chem. Phys. **98**, 1514 (1993).

[10] T. Karapiperis and B. Blankleider, Physica **78D**, 30 (1989); P. Papatzacos, Complex Systems **3**, 383 (1989).

[11] D. H. Rothman, J. Stat. Phys. **52**, 1119 (1988).

[12] J. C. Maxwell, *A Treatise on Electricity and Magnetism*, 3rd. ed. (Dover, New York, 1954), Vol. 1.

[13] R. B. Bird, W. E. Stewart, and E. N. Lightfoot, *Transport Phenomena* (John Wiley, New York, 1960).

[14] M. Sahimi and M. A. Knackstedt, J. Phys. I (France) **4**, 1269 (1994); J. P. Stokes, D. A. Weitz, J. P. Gollub, A. Dougherty, M. O. Robbins, P. M. Chaikin, and H. M. Lindsay, Phys. Rev. Lett. **57**, 1718 (1986); D. A. Weitz, J. P. Stokes, R. C. Ball, and A. P. Kushnick, Phys. Rev. Lett. **59**, 2967 (1897); J. A. M. S. Duarte, M. Sahimi and J. M. de Carvalho, J. Phys. II (France) **2**, 1 (1992).

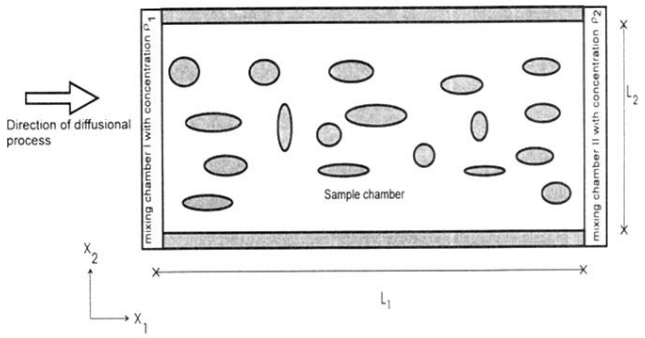

FIG. 1. Experimental setup for the estimation of effective diffusivities.

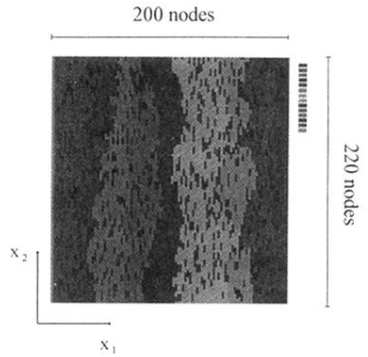

FIG. 3. Typical concentration distribution for the case of nonpermeable inclusions. Concentrations are displayed according with the scale at the right-hand side of the figure.